Molecular-Scale Structure of Uranium(VI) Immobilized with Goethite and Phosphate

ARTICLE *in* ENVIRONMENTAL SCIENCE & TECHNOLOGY · MAY 2012

Impact Factor: 5.33 · DOI: 10.1021/es300494x · Source: PubMed

4 AUTHORS, INCLUDING:

Abhas Singh
Indian Institute of Technology Kanpur
9 PUBLICATIONS **193** CITATIONS
SEE PROFILE

Jeffrey G Catalano
Washington University in St. Louis
99 PUBLICATIONS **2,091** CITATIONS
SEE PROFILE

Daniel E Giammar
Washington University in St. Louis
111 PUBLICATIONS **1,696** CITATIONS
SEE PROFILE

Environmental Science & Technology

Article

pubs.acs.org/est

Molecular-Scale Structure of Uranium(VI) Immobilized with Goethite and Phosphate

Abhas Singh,*[,†,∥] Jeffrey G. Catalano,[‡] Kai-Uwe Ulrich,[†,§] and Daniel E. Giammar[†]

[†]Department of Energy, Environmental and Chemical Engineering and [‡]Department of Earth and Planetary Sciences, Washington University, St. Louis, Missouri 63130, United States

[§]BGD Soil and Groundwater Laboratory, 01219 Dresden, Germany

[∥]Pacific Northwest National Laboratory, 902 Battelle Boulevard, Richland, Washington 99352, United States

Supporting Information

ABSTRACT: The molecular-scale immobilization mechanisms of uranium uptake in the presence of phosphate and goethite were examined by extended X-ray absorption fine structure (EXAFS) spectroscopy. Wet chemistry data from U(VI)-equilibrated goethite suspensions at pH 4−7 in the presence of ∼100 μM total phosphate indicated changes in U(VI) uptake mechanisms from adsorption to precipitation with increasing total uranium concentrations and with increasing pH. EXAFS analysis revealed that the precipitated U(VI) had a structure consistent with the meta-autunite group of solids. The adsorbed U(VI), in the absence of phosphate at pH 4−7, formed bidentate edge-sharing, ≡$Fe(OH)_2UO_2$, and bidentate corner-sharing, $(≡FeOH)_2UO_2$, surface complexes with respective U−Fe coordination distances of ∼3.45 and ∼4.3 Å. In the presence of phosphate and goethite, the relative amounts of precipitated and adsorbed U(VI) were quantified using linear combinations of the EXAFS spectra of precipitated U(VI) and phosphate-free adsorbed U(VI). A U(VI)−phosphate−Fe(III) oxide ternary surface complex is suggested as the dominant species at pH 4 and total U(VI) of 10 μM or less on the basis of the linear combination fitting, a P shell indicated by EXAFS, and the simultaneous enhancement of U(VI) and phosphate uptake on goethite. A structural model for the ternary surface complex was proposed that included a single phosphate shell at ∼3.6 Å (U−P) and a single iron shell at ∼4.3 Å (U−Fe). While the data can be explained by a U-bridging ternary surface complex, $(≡FeO)_2UO_2PO_4$, it is not possible to statistically distinguish this scenario from one with P-bridging complexes also present.

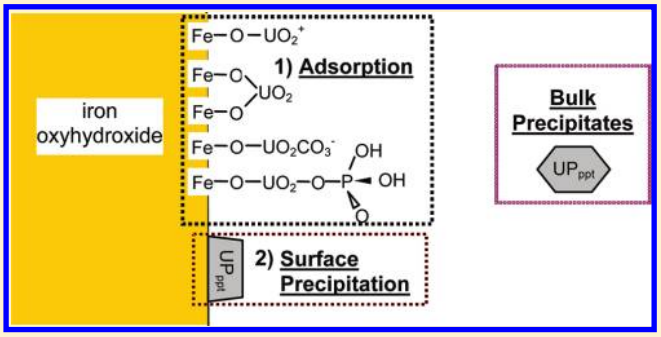

INTRODUCTION

Uranium(U) contamination of soil and groundwater is a serious environmental concern due to past mining, processing, and waste disposal activities.[1,2] Among the in situ remediation strategies for oxic subsurface environments, phosphate-induced U(VI) adsorption or precipitation as sparingly soluble uranyl phosphates can be pursued by building permeable reactive barriers of hydroxyapatite, $Ca_5(PO_4)_3(OH)_{(s)}$,[3,4] or by injecting polyphosphates.[5,6] The presence of phosphate can affect U(VI) interactions with subsurface minerals through both adsorption and precipitation mechanisms. At relatively high U(VI) and phosphate concentrations, formation of uranium phosphate solids may be important and substrate minerals such as hydroxyapatite,[4] alumina,[7] and goethite[8] may facilitate precipitation; surfaces of nonmetabolizing bacterial cell walls could even affect the size of precipitates.[9] At lower concentrations for which solutions were undersaturated with respect to uranium phosphate precipitation,[8,10,11] enhanced uptake of U(VI) on Fe(III) oxides in bench-scale studies was considered to be facilitated by the formation of inner-sphere uranyl phosphate ternary surface complexes.[8,10,11] An extended X-ray absorption fine structure (EXAFS) spectroscopy study of acidic uranium-contaminated subsurface media suggested similar ternary surface complexes.[12] However, a systematic study investigating the structure of such complexes is lacking.

Information on the coordination environment of uranium will be helpful in identifying U(VI) uptake mechanisms. Several past studies have probed the individual parts of the U(VI)−phosphate−Fe(III) oxide system at the molecular scale. These parts include U(VI) adsorption to iron oxides in phosphate-free systems, phosphate adsorption to iron oxides in U-free systems, and precipitation of uranium phosphates in the absence of iron oxides. In the absence of phosphate, at low pH, U(VI) adsorption to ferrihydrite,[13,14] hematite,[15] and goethite[16] resulted in the formation of bidentate edge-sharing (abbreviated ^{2}E) surface complexes with a U−Fe distance of ∼3.45 Å in ≡$Fe(OH)_2UO_2$. Longer U−Fe distances (∼4.0−4.2 Å) were reported for adsorbed U(VI) on a specific hematite surface ($1\bar{1}02$), consistent with the formation of bidentate

Received: February 6, 2012
Revised: May 15, 2012
Accepted: May 21, 2012
Published: May 21, 2012

corner-sharing (abbreviated ^{2}C) surface complexes.[17] For carbonate-free conditions, a recent study of U(VI) adsorption to goethite proposed a ^{2}C surface complex, ($\equiv$FeO-H)$_2$UO$_2$(H$_2$O)$_3$ (U−Fe distance ~4.3 Å), as the predominant adsorbed species.[18] The predominance of the ^{2}C complex was supported by the abundance of surface sites provided by the dominant surface of goethite.[19−21]

Phosphate adsorption to iron oxyhydroxide surfaces as inner-sphere complexes can influence U(VI)−phosphate−Fe(III) oxide interactions. From attenuated total reflectance Fourier transform infrared spectroscopy of phosphate adsorbed to goethite, both the protonated, bidentate binuclear, ($\equiv$FeO)$_2$(OH)PO, and nonprotonated, bidentate binuclear, ($\equiv$FeO)$_2$PO$_2$, inner-sphere complexes dominated at low pH (4.5), and the nonprotonated species dominated at high pH (≥7.5).[22] For ferrihydrite, only the nonprotonated species was dominant at high pH.[22,23] Phosphate adsorption can also lead to surface precipitation of an iron phosphate phase on the iron oxide surface at phosphate concentrations much lower than calculated for equilibrium with goethite and iron phosphate.[24,25]

U(VI)−phosphate precipitation could result in the formation of the meta-autunite group of solids or other uranyl phosphates depending on the prevalent groundwater chemistry.[26,27] The stability of uranyl phosphates under oxic conditions is evidenced from their occurrence in many natural[28−30] and contaminated environments.[31−36] Past studies have used EXAFS to characterize several U(VI)-phosphates; some relevant ones include chernikovite [H$_3$O(UO$_2$PO$_4$)·3H$_2$O$_{(s)}$],[4] the autunites [Ca(UO$_2$PO$_4$)$_2$·xH$_2$O$_{(s)}$],[4,37,38] sodium meta-autunite [Na$_2$(UO$_2$PO$_4$)$_2$·3H$_2$O$_{(s)}$],[39] metatorbernite [Cu(UO$_2$PO$_4$)$_2$·8H$_2$O$_{(s)}$],[37] and uranyl orthophosphate [(UO$_2$)$_3$(PO$_4$)$_2$·4H$_2$O$_{(s)}$].[37] While the first four solids listed above have the meta-autunite structure with interlayer cations between sheets of coordinated phosphate tetrahedra and uranyl square bipyramids,[26,40] the uranyl orthophosphate structure has a uranyl pentagonal bipyramid that connects the sheets of phosphate tetrahedra and uranyl pentagonal bipyramids.[41]

Our recent investigation of U(VI)−phosphate−Fe(III) oxide interactions at pH 4 indicated enhanced U uptake at high phosphate concentrations by mechanisms that depended on the total uranium (U_T) concentration.[8] While precipitation of chernikovite was dominant at U(VI) concentrations above 50 μM, for lower concentrations macroscopic observations indicated phosphate-enhanced U(VI) adsorption on goethite as the dominant uptake mechanism, and adsorption was successfully modeled by inclusion of a U(VI)−phosphate−Fe(III) oxide ternary surface complex. The objectives of this study were (1) to directly determine the changes in the U(VI) coordination environment with varying U(VI) concentrations over the low to circumneutral pH range, where phosphate amendments to U-contaminated soils are likely to be most beneficial, and (2) to spectroscopically probe for a U(VI)−phosphate−Fe(III) oxide ternary surface complex. EXAFS analysis of previously studied samples[8] equilibrated at pH 4 and newly prepared samples at pH 6 and 7 was used to distinguish between formation of ternary surface complexes and precipitation of poorly crystalline U(VI)−phosphates.

MATERIALS AND METHODS

Materials. Goethite was prepared using an established method[42] of aging initially precipitated ferrihydrite at 70 °C for 60 h. Its specific surface area is 39.9 m^2/g. Goethite was maintained as a 2.97 g/L stock suspension prior to its use in batch reactors at a diluted concentration of 0.59 g/L. All chemicals used were ACS grade or better. Ultrapure (resistivity >18.2 MΩ·cm) water was used for preparing stock solutions and dilutions. Uranium and phosphate were added from stock solutions of 1 M UO$_2$(NO$_3$)$_2$ and 0.01 M Na$_2$HPO$_4$·7H$_2$O. Buffer concentrations of 0.5 mM MES (morpholinoethanesulfonic acid) and 0.5 mM HEPES ((hydroxyethyl)-piperazineethanesulfonic acid) were used to fix the pH at 6 and 7, respectively, while no buffer was used at pH 4. Adjustments to pH were made using trace metal grade HNO$_3$ and 1 M NaOH. NaHCO$_3$ was added at pH 6 (16.2 μM) and pH 7 (64.6 μM) to yield the same inorganic carbon concentrations as when equilibrated with air ($pCO_2 = 10^{-3.44}$ atm). NaNO$_3$ was used to fix the ionic strength at 0.01 M.

Batch Experiments. Goethite samples equilibrated with a range of U_T concentrations in the absence and presence of 130 μM total phosphate (P_T) from our previous work[8] at pH 4 were collected for XAFS analysis (Table 1). Additional batch experiments were performed for 10 μM U_T at pH 6 and 7 following the same experimental protocol as for the pH 4 experiments. The pH range of 4−7 was selected because of its relevance to phosphate-based U-contamination remediation methods and to minimize confounding effects from U(VI)−carbonate complexes that are significant at higher pH.[43] The 10 U_T concentration was chosen because X-ray diffraction and electron microscopy indicated that it marked a transition in the U(VI) uptake mechanism at pH 4 from adsorption to precipitation in the presence of phosphate.[8] The P_T concentration (101 μM) for pH 6 and 7 experiments was similar to the concentration (130 μM) used for the pH 4 experiments; fresh stock solutions were prepared for the two sets of experiments. Control experiments having either no phosphate or no uranium in the presence and absence of goethite were also performed (Table S1, Supporting Information).

Table 1. U(VI)-Equilibrated Samples for EXAFS Analysis

pH	[P_T] (μM)	[U_T] (μM)	reaction time	label[a]	concn (μmol of U/g)[b]
4[c]	130	1	1 d	4GP1U1d	2
		1	1 y	4GP1U1y	2
		5	1 d	4GP5U1d	8
		10	1 y	4GP10U1y	16
		50	1 y	4GP50U1y	76
		100	1 y	4GP100U1y	125
		100	1 y	4P100U1y	goethite-free
	0	1	1 y	4G1U1y	1
		10	1 y	4G10U1y	8
		50	1 d	4G50U1d	18
		50	1 y	4G50U1y	54
		100	1 y	4G100U1y	43
6	101	10	1 y	6GP10U1y	17
	0	10		6G10U1y	17
7	101	10		7GP10U1y	17
	0	10		7G10U1y	17

[a]The first number indicates the pH, "G" indicates the presence of goethite, "P" indicates the presence of phosphate, "xU" indicates x μM U_T, "1d" or "1y" indicates the reaction time, and the absence of the letter "G" or "P" indicates goethite or phosphate, respectively, was not present. [b]Concentration per gram of goethite. [c]Macroscopic results discussed in a previous paper.[8]

dx.doi.org/10.1021/es300494x | Environ. Sci. Technol. 2012, 46, 6594−6603

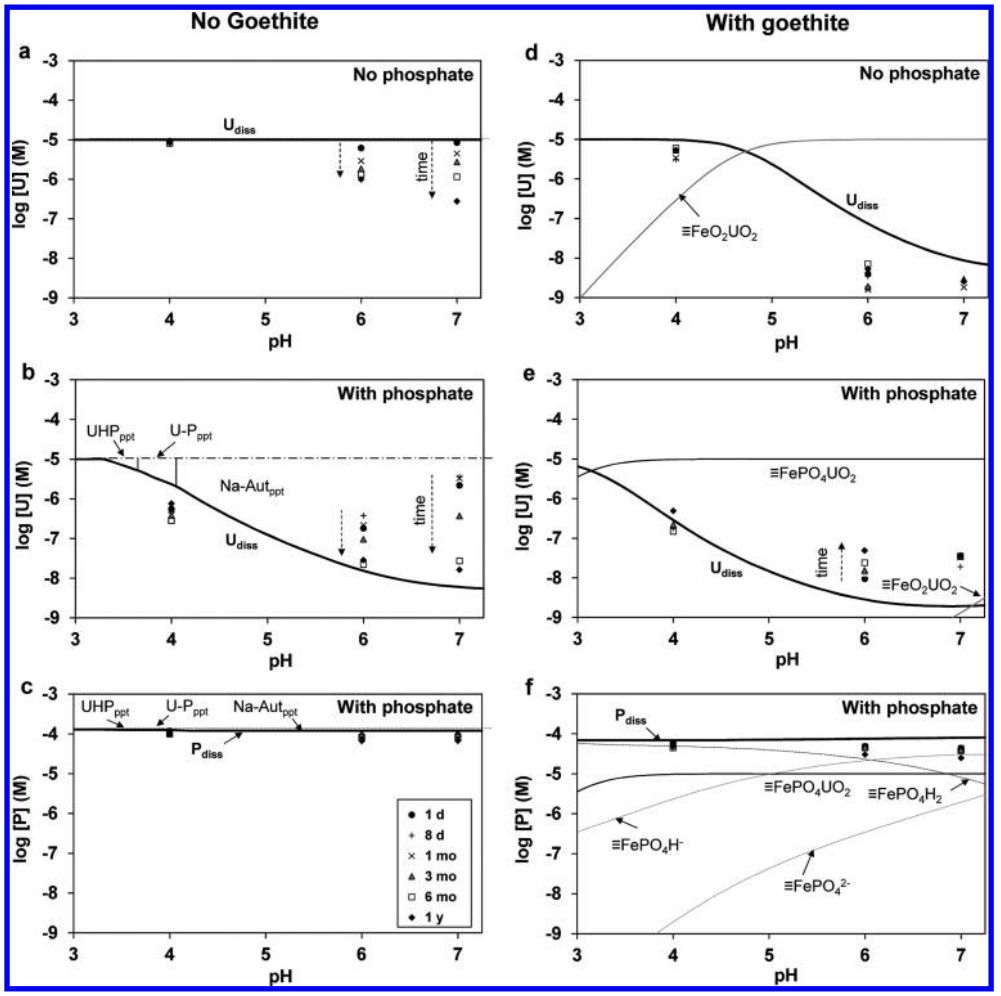

Figure 1. Predicted and measured dissolved uranium (a, b, d, e) and phosphate (c, f) concentrations in the absence (a–c) and presence (d–f) of 0.59 g/L goethite. Conditions in the absence (a, d) of phosphate are distinguished from those in phosphate's presence (b, c, e, f). The symbols represent data from 1 d to 1 y, and the lines depict equilibrium predictions for an open system with $[U_T]$ = 10 μM, $[P_T]$ = 130 μM, and $[Na_T]$ = 0.01 M. Time-dependent trends in the data are indicated by dotted arrows. Precipitates are only predicted when phosphate and U are both present in the absence of goethite. The ranges for predicted solids and predominant adsorbed species are shown. UHP_{ppt}, $U\text{-}P_{ppt}$, and $Na\text{-}Aut_{ppt}$ refer to uranium hydrogen phosphate $[UO_2HPO_4{\cdot}3H_2O_{(s)}]$, uranyl orthophosphate $[(UO_2)_3(PO_4)_2{\cdot}4H_2O_{(s)}]$, and sodium meta-autunite $[Na_2(UO_2PO_4)_2{\cdot}xH_2O_{(s)}]$, respectively. Inorganic carbon and carbonate complexation reactions were ignored in the model for clarity.

Aliquots of goethite suspensions from reactors were periodically drawn and filtered. The supernatants were analyzed for dissolved U and P concentrations by inductively coupled plasma mass spectrometry (Agilent 7500ce). Residual solids on filter membranes and solids resulting from centrifugation at 11 000 rpm for 20 min were analyzed by X-ray diffraction (XRD; Rigaku Geigerflex D-MAX/A) using Cu Kα radiation. Scanning electron microscopy (SEM) was performed using a JEOL 7001LVF. The samples after 1 d and 1 y were collected for XAFS analysis.

Sample Preparation for XAFS. U(VI)-equilibrated goethite suspensions from pH 4–7 batch experiments were centrifuged at 11 000 rpm for 20 min. The resulting wet pastes were loaded into plexiglass sample holders. Each sample holder (25.4 mm × 50.8 mm) had a well (5 mm × 5 mm × 1.5 mm) for holding the sample. The samples were sealed into the holders by wrapping with two layers of Kapton tape. The sample holders were further contained within heat-sealed polyethylene bags before being used for XAFS measurements. Uranyl nitrate and uranyl phosphate (from pH 4 experiments in the absence of goethite) standards were also analyzed by XAFS. Since these solids contained concentrated uranium, ~15 mg of uranium-containing solid was mixed with ~85 mg of boron nitride to provide appropriate total uranium concentrations for XAFS.

Structural Analysis. Molecular-scale information on U(VI) uptake mechanisms was obtained with XAFS spectroscopy. Uranium L_{III}-edge XAFS spectra were collected at room temperature on beamlines 12-BM-B[44] and 20-BM-B[45,46] at the Advanced Photon Source at Argonne National Laboratory. Both beamlines were equipped with Si(111) double-crystal monochromators. The monochromators were calibrated using a Y metal foil that was mounted between two N_2-filled ionization chambers downstream of the sample; the first inflection point in the Y K-edge was set to 17 038 eV. Spectra from the goethite-associated uranyl samples were collected in fluorescence yield and from the goethite-free uranium phosphate solids in transmission yield.[47] Fluorescence signals were collected using a 12-element solid-state Ge detector.

XAFS data were background-subtracted, splined, k^3-weighted, and processed using the Athena[48] and SIXPack[49] interfaces to the IFEFFIT XAFS analysis package.[50] Structural

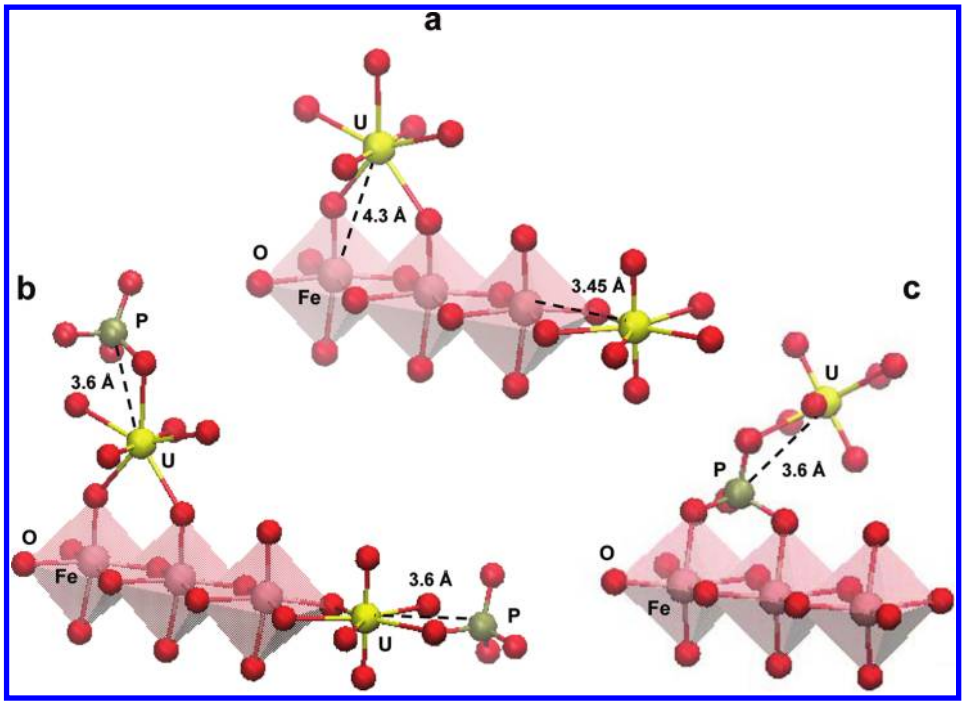

Figure 2. Structure of adsorbed uranyl along the goethite {101} surface by (a) bidentate corner-sharing (^{2}C) and bidentate edge-sharing (^{2}E) complexes in the absence of phosphate and by (b) U-bridging ^{2}C and ^{2}E and (c) P-bridging ^{2}C U(VI)−phosphate−Fe(III) oxide ternary surface complexes in the presence of phosphate. For the ^{2}C complex, the uranyl molecule is depicted with two axially bonded O atoms (parallel to the surface) and five equatorial O atoms (perpendicular to the surface) bonded to the central U atom. Note the difference in the scales among (a)−(c). This figure was prepared using VMD.[62]

fitting of the XAFS spectra was done using FEFF 8.2[51] generated phase-shift and backscattering amplitude functions from the crystal structures of sodium meta-autunite[40] and of metatorbernite[52] (with Fe substituted for Cu) over a k range of 3.5−12.4 Å^{-1} and R range of 1.2−5 Å. All fits included the three multiple scattering (MS) paths involving the axial oxygen atoms of the uranyl cation. For chernikovite spectral fitting, the MS contribution from the square equatorial oxygen shell surrounding the U atom was also included.[38] For linear combination fitting, all spectra were background-subtracted, splined, and processed in an identical manner (k = 1−12.8 Å^{-1}, R_{bkg} = 0.8, same E_0) and the edge energy was not allowed to float.

Equilibrium Speciation Calculations. Dissolved U(VI) and phosphate concentrations were predicted using the model presented previously.[8] Briefly, the model included uranium and phosphate aqueous speciation (complexation, deprotonation) reactions, dissolution−precipitation reactions, and surface complexation reactions to account for adsorption. The best available thermodynamic data and past surface complexation models were integrated to form an internally consistent framework.

RESULTS AND DISCUSSION

Macroscopic U(VI) and Phosphate Uptake. In the absence of goethite, the time-dependent decrease in measured dissolved uranium (U_{diss}) and phosphate (P_{diss}) concentrations indicated uranium phosphate precipitation for all three pH conditions (Figure 1b,c), resulting in an uptake of >95% U_T after 1 y (details in the Supporting Information). The uranium phosphate was identified as chernikovite[8] by SEM and XRD at pH 4 (SEM images of precipitates at pH 6 in Figure S5 and XRD data in Figure S6 in the Supporting Information).

In the presence of goethite, U(VI) adsorption in phosphate-free conditions increased from ∼46% of U_T at pH 4 to >99.9% of U_T at higher pH (Figure 1d). The presence of 130 μM P_T enhanced U(VI) uptake on goethite from ∼46% to ∼98% of U_T at pH 4 (Figure 1d,e). Our previous work found that, at pH 4 and 1−10 μM U_T, phosphate and U(VI) uptakes to goethite were both higher than in single-sorbate systems.[8] No evidence for precipitation was found by SEM and XRD. The simultaneous enhancement in U(VI) and phosphate uptake is consistent with the formation of U(VI)−phosphate−Fe(III) oxide ternary surface complexes.[8,10,11] Because the total phosphate uptake (∼70 μM) was much higher than the total uranium uptake (<10 μM), it is likely that phosphate also formed binary surface complexes.[8] While adsorption was the dominant U(VI) uptake mechanism at pH 4 for 10 μM U_T, U(VI)−phosphate precipitation accounted for >99% of U_T at circumneutral pH (6−7), also indicated by SEM images (Figure S7, Supporting Information) and XRD data (Figure S8, Supporting Information). At higher pH, U(VI) precipitation slightly decreased when compared to that in goethite-free conditions because dissolved phosphate was limited by adsorption to goethite (Figures 1b,c,e,f).

Molecular-Scale Characterization of U(VI) Uptake Mechanisms. EXAFS analysis yielded molecular-scale information of goethite-associated U(VI) that suggested different uptake mechanisms for different conditions. The structures of relevant end-members [(a) adsorbed U(VI) in the absence of phosphate and (b) precipitated U(VI)−phosphate in the absence of goethite] were analyzed first using shell-by-shell fitting of the corresponding Fourier-transformed EXAFS spectra. Next the ability of the EXAFS spectra of goethite-associated U(VI) with phosphate to be interpreted as a combination of these end-members was investigated using

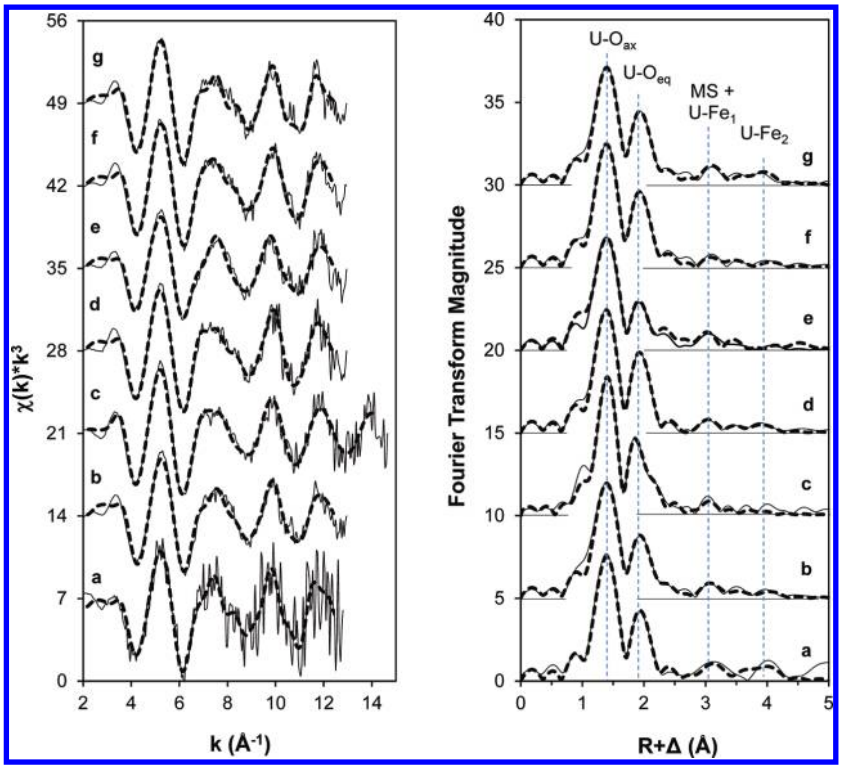

Figure 3. U L_{III}-edge EXAFS spectra (left) and Fourier transforms (right) of uranyl-sorbed goethite samples in the absence of phosphate for different pH values, U_T concentrations, and times: (a) 4G1U1y; (b) 4G10U1y; (c) 4G50U1d; (d) 4G50U1y; (e) 4G100U1y; (f) 6G10U1y; (g) 7G10U1y. Solid lines represent the data, and dashed lines represent the least-squares fits to the data. Vertical dotted lines indicate shells from the nearest neighbors and MS from the axially coordinated oxygen atoms of U. Each sample label starts with the pH, "G" indicates the presence of goethite, "*x*U" indicates *x* μM U_T, and "1d" or "1y" indicates the reaction time.

Table 2. EXAFS Fitting Results for U(VI) Adsorption to Goethite in the Absence of Phosphate[a]

sample[b]		U−O_{ax}	U−O_{eq}	U−Fe_1	U−Fe_2	ΔE_0 (eV)[c]	χ_ν^{2d}	*R* factor[e]
(a) 4G1U1y	N^f	2[i]	4(1)	0.4(2)	1.3[j]	8(2)	1.00	0.031
	R^g (Å)	1.807(7)	2.40(2)	3.47(4)	4.33(2)			
	$\sigma^{2\,h}$ (Å^2)	0.0017(5)	0.008(3)	0.003(2)	0.003[j]			
(b) 4G10U1y	N^f	2[i]	4(1)	0.4(3)	1.2[j]	10(2)	15.51	0.025
	R^g (Å)	1.802(7)	2.3(2)	3.42(6)	4.31(4)			
	$\sigma^{2\,h}$ (Å^2)	0.0025(5)	0.009(9)	0.008(4)	0.008[j]			
(c) 4G50U1d	N^f	2[i]	6(1)	0.8(5)	0.5[j]	6(1)	2.33	0.021
	R^g (Å)	1.799(5)	2.40(1)	3.35(5)	4.2(2)			
	$\sigma^{2\,h}$ (Å^2)	0.0019(3)	0.012(2)	0.012(7)	0.012[j]			
(d) 4G50U1y	N^f	2[i]	4.1(5)	0.4(2)	1.3[j]	6.9(8)	2.53	0.008
	R^g (Å)	1.802(3)	2.400(6)	3.35(4)	4.26(2)			
	$\sigma^{2\,h}$ (Å^2)	0.0019(3)	0.007(1)	0.008(2)	0.008[j]			
(e) 4G100U1y	N^f	2[i]	5(3)	0.6(3)	1.3[j]	7(3)	12.31	0.031
	R^g (Å)	1.802(9)	2.41(3)	3.44(5)	4.26(2)			
	$\sigma^{2\,h}$ (Å^2)	0.0023(5)	0.017(8)	0.008(4)	0.008[j]			
(f) 6G10U1y	N^f	2[i]	4.4(7)		0.9(7)[k]	8(1)	9.74	0.014
	R^g (Å)	1.800(4)	2.396(9)		4.31(4)			
	$\sigma^{2\,h}$ (Å^2)	0.0019(3)	0.008(2)		0.008[i]			
(g) 7G10U1y	N^f	2[i]	5(1)	0.4(2)	1.1[j]	8(2)	15.19	0.028
	R^g (Å)	1.804(7)	2.41(2)	3.45(3)	4.28(3)			
	$\sigma^{2\,h}$ (Å^2)	0.0023(5)	0.009(3)	0.004(2)	0.004[j]			

[a]The estimated standard deviations are listed in parentheses, representing errors in the last digit; the amplitude damping factor, $S_o^2 = 1$, was used for all fits. [b]The first number indicates the pH, "G" indicates the presence of goethite, "*x*U" indicates *x* μM U_T, and "1d" or "1y" indicates the reaction time. [c]Difference in threshold Fermi levels between the data and theory. [d]Reduced χ^2 as a goodness-of-fit parameter. [e]*R* factor as a goodness-of-fit parameter. [f]Coordination number. [g]Interatomic distance. [h]Debye−Waller factor. [i]Fixed parameter during fitting. [j]Linked parameter during fitting. [k]Only one Fe shell was fit because *N* for the shorter Fe shell always refined to nearly zero.

linear combination (LC) fitting. For LC fitting of EXAFS spectra the end-members should be 100% pure in terms of their molecular-scale structure. For conditions where the LC fitting suggested contributions from an end-member that could not be

dx.doi.org/10.1021/es300494x | Environ. Sci. Technol. 2012, 46, 6594−6603

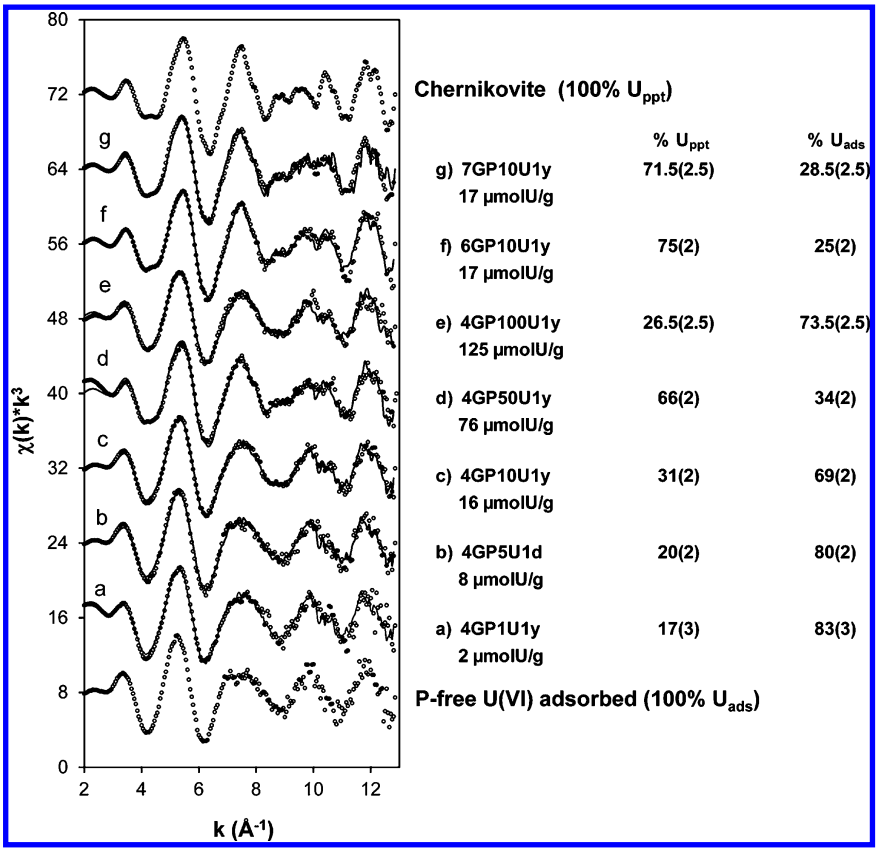

Figure 4. Two-component linear combination fits (solid lines) to the EXAFS spectra (dotted lines) of goethite-associated U(VI) samples in the presence of ~100 μM total phosphate. The end-members are shown at the top and bottom of the figure. Also shown are the percentages of adsorbed and precipitated uranium predicted by the fitting. The P-free end-member shown is a representative spectrum of U(VI) adsorbed to goethite corresponding to the 50 μM U_T condition (4G50U1d). While fitting, the spectrum for adsorbed U(VI) for each U_T condition and pH was chosen as the end-member. The estimated standard deviations are listed in parentheses, representing errors in the last digit (last two digits for spectra e and g). Each sample label starts with the pH, "G" indicates the presence of goethite, "P" indicates the presence of phosphate, "xU" indicates x μM U_T, and "1d" or "1y" indicates the reaction time.

present (e.g., U(VI)−phosphate precipitate at undersaturated conditions), changes to the average EXAFS spectra were examined in greater detail by shell-by-shell fitting that pointed to the formation of U(VI)−phosphate−Fe(III) oxide ternary surface complexes.

U(VI) Adsorption in the Absence of Phosphate. U(VI) adsorbed to the goethite surface by forming ^{2}E[16] and ^{2}C[18] inner-sphere binary surface complexes (Figure 2a). Features in EXAFS spectra and the corresponding Fourier transforms for uranyl-sorbed goethite samples indicative of different oxygen and Fe shells were used to determine the structures of the binary surface complexes (Figure 3). U(VI) adsorption to goethite for low to circumneutral pH (4−7) conditions was modeled by using a structural model that included a single axial oxygen shell at ~1.78 Å (U−O_{ax}), a single equatorial oxygen shell at ~2.4 Å (U−O_{eq}), the three multiple scattering paths associated with U−O_{ax}, and two iron shells at ~3.45 Å (U−Fe_1) and ~4.3 Å (U−Fe_2) (Table 2). The coordination numbers (N_i) for the two iron shells were constrained to obtain structurally reasonable fits resulting from reduced correlations in coordination number and Debye−Waller parameters. Because a ^{2}E surface complex has one Fe neighbor (U−Fe_1) and a ^{2}C surface complex has two Fe neighbors (U−Fe_2), the N values were related to the fractional coverage of the complexes as

$$N_{\text{U-Fe}_1} + 0.5N_{\text{U-Fe}_2} = 1 \quad (1)$$

Past studies of U(VI) adsorption on iron oxide surfaces have attributed the ~3 Å (uncorrected for phase shift) Fourier transform feature either entirely to the multiple scattering related to the U−O_{ax} shell[18] or to U−O_{ax} multiple scattering and a ^{2}E inner-sphere complex.[13,15,43] For our spectra both the U−O_{ax} multiple scattering and the ^{2}E complex were required to fit this feature (details in the Supporting Information). Furthermore, the Fourier transform feature at ~4.0 Å could be interpreted by including a second iron shell resulting from the recently proposed ^{2}C binary surface complex.[17,18] Depending on the goethite surface morphology and the relative abundance of surfaces favoring the two complexes, both the ^{2}E and ^{2}C complexes could be significant in explaining the high sorption capacity of goethite. In our model, no U−C paths were included because uranyl carbonate surface complexes were not expected to be significant for the pH and pCO_2 conditions investigated.[43] Some previous studies have accounted for the effect of carbonate on U(VI) adsorption by a U(VI)−CO_3 ternary surface complex even at low pH.[15,53] However, a recent study elucidated that uranium carbonate surface complexes on ferrihydrite were dominant only at high pH and elevated pCO_2 levels by using advanced EXAFS iterative transformation factor analysis and surface complexation modeling for a range of pH and pCO_2 conditions.[43]

dx.doi.org/10.1021/es300494x | Environ. Sci. Technol. 2012, 46, 6594−6603

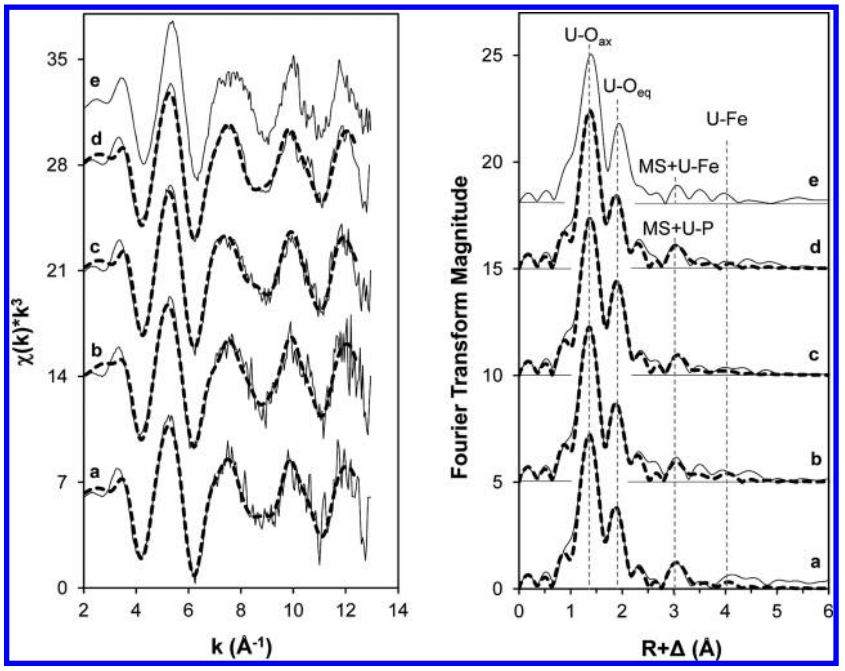

Figure 5. U L_{III}-edge EXAFS spectra (left) and Fourier transforms (right) of uranyl-sorbed goethite samples in the presence of phosphate at pH 4 for different U_T concentrations and times: (a) 4GP1U1d; (b) 4GP1U1y; (c) 4GP5U1d; (d) 4GP10U1y. Spectrum e represents the phosphate-free condition (4G10U1y) analogous to spectrum d. Solid lines represent the data, and dashed lines represent the least-squares fits to the data. Vertical dotted lines indicate shells from the nearest neighbors and MS from the axially coordinated oxygen atoms of U. Each sample label starts with the pH, "G" indicates the presence of goethite, "P" indicates the presence of phosphate, "*x*U" indicates *x* μM U_T, and "1d" or "1y" indicates the reaction time.

U(VI)−Phosphate Precipitation in the Absence of Goethite. A U(VI)−phosphate (chernikovite) precipitated at pH 4 for intermediate (10 μM) to high (100 μM) U_T concentrations[8] was used as an end-member for evaluating relative contributions of precipitation and adsorption in subsequent samples. The formation of a meta-autunite group mineral (e.g., chernikovite), determined previously by XRD and SEM,[8] was also confirmed by XAFS (Figure S2, Supporting Information); the experimental spectrum was successfully fit (Table S4, Supporting Information) to a meta-autunite sheet structure.[40] The meta-autunite structures have sheets of coordinated uranium and phosphate polyhedra with interlayer cations.[26] EXAFS cannot clearly identify the interlayer cation in the meta-autunites and is only sensitive to the overall sheet structure.[37] U(VI)−phosphate precipitation was also found for the 10 μM U_T conditions at pH 6 and 7 and confirmed by SEM (Figure S5, Supporting Information).

Phosphate-Induced U(VI) Uptake in the Presence of Goethite. U(VI) adsorption on goethite was the dominant mechanism for U(VI) uptake in the presence of phosphate at pH 4 for low to intermediate U_T concentrations ($\leq$10 μM), while chernikovite precipitation was the predominant mode of U(VI) uptake for higher concentrations.[8] To quantify the relative amounts of adsorbed and precipitated U(VI) for different U_T concentrations and pH values, the EXAFS spectra corresponding to these uranium-associated goethite samples (Figure 4) were fitted using LCs of the spectra of chernikovite and phosphate-free uranyl-sorbed goethite.

At pH 4 the LC fitting indicates the presence of U(VI) in both adsorbed and precipitated forms. At $U_T \leq 5$ μM, uranium was predominantly present in an adsorbed form. With increasing U_T concentrations, the percentages of precipitated U increased until the 50 μM U_T concentration (Figure 4a−d). However, with a further increase in U_T concentration to 100 μM, the percentage of precipitated U decreased (Figure 4e) because the dissolved phosphate that remained (~60 μM) after phosphate adsorption to the goethite was insufficient to precipitate as much uranium as it did for the 50 μM U_T concentration.[8] An increase in pH from 4 to 6 or 7 at a fixed U_T concentration (10 μM) caused the predominant mechanism to change from adsorption (69%) to precipitation (72−75%, Figure 4f,g). The spectra for conditions with 66−75% precipitation (Figure 4d,f,g) closely resemble the meta-autunite end-member spectrum.

LC fitting results qualitatively agree with macroscopic uptake results for the high U_T concentrations at pH 4 and for the circumneutral pH conditions discussed previously. For the low to intermediate U_T concentrations ($\leq$10 μM) at pH 4, however, no evidence for precipitation was found from XRD and SEM[8] even when LC fitting results indicated 17−30% precipitation (Figure 4a−c). The equilibrated solutions were undersaturated with respect to chernikovite, sodium meta-autunite, and uranyl orthophosphate (the saturation indices $[\log(Q/K_{sp})]$ for the 10 μM U_T concentration after 1 y were −1.05, −0.975, and −2.37, respectively). The effect of a single monodentate P shell on the EXAFS spectrum, as in a ternary complex, may produce a spectrum similar to an LC of an autunite spectrum and the spectrum of U-sorbed goethite. It is difficult to distinguish the two cases. At conditions where no uranyl phosphate precipitate appears to have formed, the need to include an autunite component in the model suggests the presence of a ternary complex or at least that phosphate is coordinating with U. Such a ternary surface complex has been previously used in surface complexation models describing phosphate-enhanced U(VI) uptake on iron oxides.[8,10,11]

Structure of the U(VI)−Phosphate−Fe(III) Oxide Ternary Surface Complex. Although formation of a ternary surface complex has been hypothesized,[8,10−12] definitive evidence of its

dx.doi.org/10.1021/es300494x | *Environ. Sci. Technol.* 2012, 46, 6594−6603

Table 3. EXAFS Fitting Results for Spectra of U(VI)-Sorbed Goethite in the Presence of Phosphate[a]

sample[b]		U−O_{ax}	U−$O_{eq\ 1}$	U−$O_{eq\ 2}$	U−P	U−Fe	ΔE_0[c] (eV)	χ_ν^{2}[d]	R factor[e]
(a) 4GP1U1d	N[f]	2[i]	3.0(5)	1.7(6)	1.0(5)	0.7(9)	4(2)	6.75	0.019
	R(Å)[g]	1.782(8)	2.31(3)	2.46(5)	3.60(3)	4.32(7)			
	σ^2(Å^2)[h]	0.0023(4)	0.005[i]	0.005[j]	0.005[i]	0.008[i]			
(b) 4GP1U1y	N[f]	2[i]	2.8(6)	1.8(7)	0.4(7)	1(1)	6(2)	6.25	0.040
	R(Å)[g]	1.784(9)	2.34(3)	2.50(5)	3.61(1)	4.30(6)			
	σ^2(Å^2)[h]	0.0022(6)	0.005[i]	0.005[j]	0.005[i]	0.008[i]			
(c) 4GP5U1d	N[f]	2[i]	3.2(6)	1.6(6)	0.5(5)	0.2(8)	7(2)	9.11	0.017
	R(Å)[g]	1.792(8)	2.34(3)	2.48(6)	3.60(6)	4.2(2)			
	σ^2(Å^2)[h]	0.0027(6)	0.005[i]	0.005[j]	0.005[i]	0.008[i]			
(d) 4GP10U1y	N[f]	2[i]	2.9(4)	1.9(5)	0.8(5)	0.4(9)	6(2)	51.27	0.021
	R(Å)[g]	1.787(8)	2.31(3)	2.47(4)	3.61(4)	4.3(1)			
	σ^2(Å^2)[h]	0.0020(4)	0.005[i]	0.005[j]	0.005[i]	0.008[i]			

[a]The estimated standard deviations are listed in parentheses, representing errors in the last digit; the amplitude damping factor, $S_o^2 = 1$, was used for all fits. [b]The first number indicates the pH, "G" indicates the presence of goethite, "P" indicates the presence of phosphate, "xU" indicates x μM U_T, and "1d" or "1y" indicates the reaction time. [c]Difference in threshold Fermi levels between the data and theory. [d]Reduced χ^2 as a goodness-of-fit parameter. [e]R factor as a goodness-of-fit parameter. [f]Coordination number. [g]Interatomic distance. [h]Debye−Waller factor. [i]Fixed parameter during fitting. [j]Linked parameter during fitting.

structure is lacking.[12] The EXAFS spectra and corresponding Fourier transforms of goethite samples with U(VI) adsorbed in the presence of phosphate at pH 4 for 1−10 μM U_T were best fit (Figure 5) from a structural model that included a single axial oxygen shell at ∼1.78 Å (U−O_{ax}), a split equatorial oxygen shell at ∼2.3 Å (U−$O_{eq\ 1}$) and ∼2.5 Å (U−$O_{eq\ 2}$), the three multiple scattering paths associated with U−O_{ax}, a single phosphorus shell at ∼3.6 Å (U−P), and a single iron shell at ∼4.3 Å (U−Fe) (Table 3). The presence of phosphate alters U(VI) EXAFS spectra in two regions of the Fourier transforms, between 1.7 and 2.5 Å and around 3.0 Å (Figure S3, Supporting Information, explains model development in detail), consistent with what is expected for monodentate phosphate complexation. The simultaneous enhancement in U(VI) and phosphate uptake from wet chemistry data strongly suggests that most of the U is in a ternary surface complex and other U species, such as P-free adsorbed U(VI), are almost negligible in comparison. The dominance of the ternary surface complex is also supported by the good fit to dissolved U and P data with a surface complexation model.[8]

While there is definitive evidence for the formation of a ternary surface complex, its exact structure cannot be determined. Although the fitting of a U−P shell at 3.6 Å and of a U−Fe shell at 4.3 Å suggests a U-bridging ^{2}C ternary surface complex (Figure 2b), it is not possible to statistically distinguish this scenario from one where only P-bridging complexes (Figure 2c) or a combination of U-bridging and P-bridging complexes were present. The fitting of a U−Fe shell at 4.3 Å with $N_{U-Fe2} < 2$ (Table 3) improves the quality of fit but does not prove its existence because N_{U-Fe2} is within an error of 0. Furthermore, because of the uncertainty in the spectral contribution of the shorter U−Fe shell (which overlaps the U−P shell), definite conclusions regarding the existence of any U-bridging ^{2}E ternary surface complexes (Figure 2b) also cannot be drawn (details in the Supporting Information). U(VI) adsorption as a U-bridging ternary surface complex has been suggested previously on different sorbates, in a monodentate U−P coordination on contaminated soils from three U. S. Department of Energy (U.S. DOE) nuclear waste sites[12] and in predominantly bidentate U−P coordination on hydroxyapatite surfaces (except for one condition where it was monodentate).[4] Likewise, a recent time-resolved vibrational spectroscopy study of U(VI)−ferrihydrite−carbonate systems for the pH range 5.5−8 indicated U(VI) adsorption as U-bridging ^{2}E ternary surface complexes[54] previously suggested by EXAFS[43,55] and surface complexation modeling[56] studies.

For our year-long study the order of addition of phosphate and uranium should have no impact on the final speciation because equilibrium will only depend on the total inputs to the system. Both P-bridging and U-bridging ternary surface complexes could form. At equilibrium, phosphate and uranium are constantly adsorbing and desorbing, and sites will be available for U(VI) sorption if that situation is energetically more favorable. Previous studies of phosphate reactions with goethite surfaces in the absence of any adsorbate[24,25] proposed the development of a 2-dimensional Fe(III)−phosphate phase at surface coverages exceeding a critical value (210−235 μmol/g at pH < 4.42); however, this critical value was well above the conditions in the present study (120−140 μmol/g at pH 4).

Environmental Implications. This study demonstrates that phosphate-induced uranium adsorption and precipitation processes co-occur under a wider range of conditions than investigated previously. These conditions include the low to circumneutral pH range, over which phosphate addition is likely to have the most benefit for remediation. Together with recent findings about the importance of phosphate on U(IV) immobilization mechanisms,[57,58] products,[59,60] and stability,[59,61] this research highlights the potentially important role of phosphate on uranium fate for both U(VI) and U(IV). Phosphate's impact in immobilizing U(VI) involves more than just precipitation, as it enables U(VI) adsorption via formation of U(VI)−phosphate−Fe(III) oxide ternary surface complexes. The long-term stability for adsorbed versus precipitated uranium may be different. Because adsorbed U(VI) is only at mineral surfaces and desorption rates can be controlled by diffusion, it is likely that adsorbed U(VI) will be more labile.

This study suggests a U-bridging $(\equiv FeO)_2UO_2PO_4$ structure of the ternary surface complex, but it is also statistically possible that a P-bridging structure was present. Additional structural information could be useful for setting reaction stoichiometries in surface complexation models that predict adsorption to soils or sediments and are then incorporated into reactive transport models. Furthermore,

while ternary surface complexes were clearly identified at pH 4 and a surface complexation model predicts their occurrence at higher pH, their existence under circumneutral and alkaline conditions needs spectroscopic confirmation. Such conditions are potentially more relevant to the environment, especially to groundwater systems near saturation with calcite.

■ ASSOCIATED CONTENT

Supporting Information

Details on the experimental conditions, macroscopic observations, and structural model development. This material is available free of charge via the Internet at http://pubs.acs.org.

■ AUTHOR INFORMATION

Corresponding Author

*Phone: (509) 371-7370, fax: (509) 371-6354, e-mail: abhas.singh@pnnl.gov.

Notes

The authors declare no competing financial interest.

■ ACKNOWLEDGMENTS

This research was supported by the National Science Foundation (Grant BES 0608749). The Center for Materials Innovation at Washington University provided partial funding. K.-U.U.'s contribution was supported by the Office of Science (Biological and Environmental Research), U.S. DOE (Grant DE-FG02-06ER64229). J.G.C. gratefully acknowledges support from the U.S. DOE's Subsurface Biogeochemical Research Program (Grant DE-SC0006857). Pacific Northwest Consortium/X-ray Science Division facilities at the Advanced Photon Source, and research at these facilities, are supported by the U.S. DOE–Basic Energy Sciences, a Major Resources Support grant from the Natural Sciences and Engineering Research Council of Canada, the University of Washington, Simon Fraser University, and the Advanced Photon Source (APS). Use of the APS, an Office of Science User Facility operated for the U.S. DOE by Argonne National Laboratory, was supported under Contract DE-AC02-06CH11357. We thank Dr. Sebastian N. Kerisit at Pacific Northwest National Laboratory for his help in making the structural figures and Dr. Michelle M. Scherer and the three anonymous reviewers whose inputs helped considerably improve this manuscript.

■ REFERENCES

(1) Riley, R. G.; Zachara, J. M. *Chemical Contaminants on DOE Lands and Selection of Contaminant Mixtures for Subsurface Science Research*; DOE/ER-0547T; U.S. Department of Energy, Office of Energy Research: Washington, DC, 1992.

(2) U.S. DOE. *Linking Legacies: Connecting Cold War Nuclear Weapons Processes to Their Environmental Consequences*; U.S. Department of Energy, Office of Environmental Management: Washington, DC, 1997.

(3) Arey, J. S.; Seaman, J. C.; Bertsch, P. Immobilization of uranium in contaminated sediments by hydroxyapatite addition. *Environ. Sci. Technol.* **1999**, *33* (2), 337–342.

(4) Fuller, C. C.; Bargar, J. R.; Davis, J. A.; Piana, M. J. Mechanisms of uranium interactions with hydroxyapatite: Implications for groundwater remediation. *Environ. Sci. Technol.* **2002**, *36* (2), 158–165.

(5) Vermuel, V. R.; Fruchter, J. S.; Wellman, D. M.; Williams, B. A.; Williams, M. D. *Site Characterization Plan: Uranium Stabilization through Polyphosphate Injection—300 Area Uranium Plume Treatability Demonstration Project*; PNNL-16008; Pacific Northwest National Laboratory: Richland, WA, 2006.

(6) Wellman, D. M.; Pierce, E. M.; Richards, E. L.; Butler, B. C.; Parker, K. E.; Glovack, J. N.; Burton, S. D.; Baum, S. R.; Clayton, E. T.; Rodriguez, E. A. *Interim Report: Uranium Stabilization through Polyphosphate Injection—300 Area Uranium Plume Treatability Demonstration Project*; PNNL-16683; Environmental Molecular Sciences Laboratory, Pacific Northwest National Laboratory, Richland, WA, 2007.

(7) Del Nero, M.; Galindo, C.; Barillon, R. m.; Madé, B. TRLFS evidence for precipitation of uranyl phosphate on the surface of alumina: Environmental implications. *Environ. Sci. Technol.* **2011**, *45* (9), 3982–3988.

(8) Singh, A.; Ulrich, K.-U.; Giammar, D. E. Impact of phosphate on U(VI) immobilization in the presence of goethite. *Geochim. Cosmochim. Acta* **2010**, *74* (22), 6324–6343.

(9) Dunham-Cheatham, S.; Rui, X.; Bunker, B.; Menguy, N.; Hellmann, R.; Fein, J. The effects of non-metabolizing bacterial cells on the precipitation of U, Pb and Ca phosphates. *Geochim. Cosmochim. Acta* **2011**, *75* (10), 2828–2847.

(10) Cheng, T.; Barnett, M. O.; Roden, E. E.; Zhuang, J. L. Effects of phosphate on uranium(VI) adsorption to goethite-coated sand. *Environ. Sci. Technol.* **2004**, *38* (22), 6059–6065.

(11) Payne, T. E.; Davis, J. A.; Waite, T. D. Uranium adsorption on ferrihydrite—Effects of phosphate and humic acid. *Radiochim. Acta* **1996**, *74*, 239–243.

(12) Bostick, B. C.; Fendorf, S.; Barnett, M. O.; Jardine, P. M.; Brooks, S. C. Uranyl surface complexes formed on subsurface media from DOE facilities. *Soil Sci. Soc. Am. J.* **2002**, *66* (1), 99–108.

(13) Waite, T. D.; Davis, J. A.; Payne, T. E.; Waychunas, G. A.; Xu, N. Uranium (VI) adsorption to ferrihydrite: Application of a surface complexation model. *Geochim. Cosmochim. Acta* **1994**, *58* (24), 5465–5478.

(14) Ulrich, K.-U.; Rossberg, A.; Foerstendorf, H.; Zänker, H.; Scheinost, A. C. Molecular characterization of uranium (VI) sorption complexes on iron (III)-rich acid mine water colloids. *Geochim. Cosmochim. Acta* **2006**, *70* (22), 5469–5487.

(15) Bargar, J. R.; Reitmeyer, R.; Davis, J. A. Spectroscopic confirmation of uranium (VI)–carbonato adsorption complexes on hematite. *Environ. Sci. Technol.* **1999**, *33* (14), 2481–2484.

(16) Moyes, L. N.; Parkman, R. H.; Charnock, J. M.; Vaughan, D. J.; Livens, F. R.; Hughes, C. R.; Braithwaite, A. Uranium uptake from aqueous solution by interaction with goethite, lepidocrocite, muscovite, and mackinawite: An X-ray absorption spectroscopy study. *Environ. Sci. Technol.* **2000**, *34* (6), 1062–1068.

(17) Catalano, J. G.; Trainor, T. P.; Eng, P. J.; Waychunas, G. A.; Brown, G. E., Jr. CTR diffraction and grazing-incidence EXAFS study of U(VI) adsorption onto α-Al_2O_3 and α-Fe_2O_3 $(1\bar{1}02)$ surfaces. *Geochim. Cosmochim. Acta* **2005**, *69* (14), 3555–3572.

(18) Sherman, D. M.; Peacock, C. L.; Hubbard, C. G. Surface complexation of U (VI) on goethite (α-FeOOH). *Geochim. Cosmochim. Acta* **2008**, *72* (2), 298–310.

(19) Boily, J. F.; Lützenkirchen, J.; Balmès, O.; Beattie, J.; Sjöberg, S. Modeling proton binding at the goethite (α-FeOOH)-water interface. *Colloids Surf., A* **2001**, *179* (1), 11–27.

(20) Randall, S. R.; Sherman, D. M.; Ragnarsdottir, K. V.; Collins, C. R. The mechanism of cadmium surface complexation on iron oxyhydroxide minerals. *Geochim. Cosmochim. Acta* **1999**, *63* (19–20), 2971–2987.

(21) Schwertmann, U.; Murad, E. Effect of pH on the formation of goethite and hematite from ferrihydrite. *Clays Clay Miner.* **1983**, *31* (4), 277–284.

(22) Luengo, C.; Brigante, M.; Antelo, J.; Avena, M. Kinetics of phosphate adsorption on goethite: Comparing batch adsorption and ATR-IR measurements. *J. Colloid Interface Sci.* **2006**, *300* (2), 511–518.

(23) Arai, Y.; Sparks, D. L. ATR-FTIR spectroscopic investigation on phosphate adsorption mechanisms at the ferrihydrite-water interface. *J. Colloid Interface Sci.* **2001**, *241* (2), 317–326.

(24) Ler, A.; Stanforth, R. Evidence for surface precipitation of phosphate on goethite. *Environ. Sci. Technol.* **2003**, *37* (12), 2694−2700.
(25) Li, L.; Stanforth, R. Distinguishing adsorption and surface precipitation of phosphate on goethite (α-FeOOH). *J. Colloid Interface Sci.* **2000**, *230* (1), 12−21.
(26) Finch, R.; Murakami, T. Systematics and paragenesis of uranium minerals. In *Uranium: Mineralogy, Geochemistry and the Environment*; Burns, P. C., Finch, R., Eds.; Mineralogical Society of America: Washington, DC, 1999; Vol. *38*, pp 91−180.
(27) Guillaumont, R.; Fanghänel, T.; Fuger, J.; Grenthe, I.; Neck, V.; Palmer, D. A.; Rand, M. H. *Update on the Chemical Thermodynamics of Uranium, Neptunium, Plutonium, Americium, and Technetium*; OECD Nuclear Energy Agency, Ed.; Elsevier: Amsterdam, 2003.
(28) Murakami, T.; Sato, T.; Ohnuki, T.; Isobe, H. Field evidence for uranium nanocrystallization and its implications for uranium transport. *Chem. Geol.* **2005**, *221* (1−2), 117−126.
(29) Sato, T.; Murakami, T.; Yanase, N.; Isobe, H.; Payne, T. E.; Airey, P. L. Iron nodules scavenging uranium from groundwater. *Environ. Sci. Technol.* **1997**, *31* (10), 2854−2858.
(30) Jerden, J. L.; Sinha, A. K. Phosphate based immobilization of uranium in an oxidizing bedrock aquifer. *Appl. Geochem.* **2003**, *18* (6), 823−843.
(31) Arai, Y.; Marcus, M. K.; Tamura, N.; Davis, J. A.; Zachara, J. M. Spectroscopic evidence for uranium bearing precipitates in vadose zone sediments at the Hanford 300-area site. *Environ. Sci. Technol.* **2007**, *41* (13), 4633−4639.
(32) Buck, E. C.; Brown, N. R.; Dietz, N. L. Contaminant uranium phases and leaching at the Fernald site in Ohio. *Environ. Sci. Technol.* **1996**, *30* (1), 81−88.
(33) Catalano, J. G.; McKinley, J. P.; Zachara, J. M.; Heald, S. M.; Smith, S. C.; Brown, G. E. Changes in uranium speciation through a depth sequence of contaminated Hanford sediments. *Environ. Sci. Technol.* **2006**, *40* (8), 2517−2524.
(34) Morris, D. E.; Allen, P. G.; Berg, J. M.; Chisholm-Brause, C. J.; Conradson, S. D.; Donohoe, R. J.; Hess, N. J.; Musgrave, J. A.; Tait, C. D. Speciation of uranium in Fernald soils by molecular spectroscopic methods: Characterization of untreated soils. *Environ. Sci. Technol.* **1996**, *30* (7), 2322−2331.
(35) Roh, Y.; Lee, S. R.; Choi, S.-K.; Elless, M. P.; Lee, S. Y. Physicochemical and mineralogical characterization of uranium-contaminated soils. *Soil Sediment Contam.* **2000**, *9* (5), 463−486.
(36) Stubbs, J. E.; Veblen, L. A.; Elbert, D. C.; Zachara, J. M.; Davis, J. A.; Veblen, D. R. Newly recognized hosts for uranium in the Hanford site vadose zone. *Geochim. Cosmochim. Acta* **2009**, *73* (6), 1563−1576.
(37) Catalano, J. G.; Brown, G. E., Jr. Analysis of uranyl-bearing phases by EXAFS spectroscopy: Interferences, multiple scattering, accuracy of structural parameters, and spectral differences. *Am. Mineral.* **2004**, *89* (7), 1004.
(38) Thompson, H. A.; Brown, G. E.; Parks, G. A. XAFS spectroscopic study of uranyl coordination in solids and aqueous solution. *Am. Mineral.* **1997**, *82* (5−6), 483−496.
(39) Wellman, D. M.; Catalano, J. G.; Icenhower, J. P.; Gamerdinger, A. P. Synthesis and characterization of sodium meta-autunite, $Na[UO_2PO_4]\cdot 3H_2O$. *Radiochim. Acta* **2005**, *93* (7), 393−399.
(40) Locock, A. J.; Burns, P. C.; Duke, M. J. M.; Flynn, T. M. Monovalent cations in structures of the meta-autunite group. *Can. Mineral.* **2004**, *42* (4), 973.
(41) Locock, A. J.; Burns, P. C. The crystal structure of triuranyl diphosphate tetrahydrate. *J. Solid State Chem.* **2002**, *163* (1), 275−280.
(42) Schwertmann, U.; Cornell, R. M. *The Iron Oxides: Structure, Properties, Reactions, Occurrences and Uses*, 2nd ed.; Wiley-VCH: New York, 2003.
(43) Rossberg, A.; Ulrich, K.-U.; Weiss, S.; Tsushima, S.; Hiemstra, T.; Scheinost, A. C. Identification of uranyl surface complexes on ferrihydrite: Advanced EXAFS data analysis and CD-MUSIC modeling. *Environ. Sci. Technol.* **2009**, *43* (5), 1400−1406.
(44) Beno, M. A.; Engbretson, M.; Jennings, G.; Knapp, G. S.; Linton, J.; Kurtz, C.; Rütt, U.; Montano, P. A. BESSRC-CAT bending magnet beamline at the advanced photon source. *Nucl. Instrum. Methods Phys. Res., Sect. A* **2001**, *467*, 699−702.
(45) Heald, S. M. Optics upgrades at the APS beamline 20-BM. *Nucl. Instrum. Methods Phys. Res., Sect. A* **2011**, *649* (1), 128−130.
(46) Heald, S. M.; Brewe, D. L.; Stern, E. A.; Kim, K. H.; Brown, F. C.; Jiang, D. T.; Crozier, E. D.; Gordon, R. A. XAFS and micro-XAFS at the PNC-CAT beamlines. *J. Synchrotron Radiat.* **1999**, *6* (3), 347−349.
(47) Kelly, S. D., Hesterberg, D., Ravel, B. *Analysis of Soils and Minerals Using X-ray Absorption Spectroscopy. Methods of Soil Analysis, Part 5—Mineralogical Methods*; Soil Science Society of America: Madison, WI, 2008; pp 367−463.
(48) Ravel, B.; Newville, M. ATHENA, ARTEMIS, HEPHAESTUS: Data analysis for X-ray absorption spectroscopy using IFEFFIT. *J. Synchrotron Radiat.* **2005**, *12* (4), 537−541.
(49) Webb, S. M. SIXPACK: A graphical user interface for XAS analysis using IFEFFIT. *Phys. Scr.* **2005**, *115*, 1011−1014.
(50) Newville, M. IFEFFIT: Interactive XAFS analysis and FEFF fitting. *J. Synchrotron Radiat.* **2001**, *8* (2), 322−324.
(51) Ankudinov, A. L.; Bouldin, C. E.; Rehr, J. J.; Sims, J.; Hung, H. Parallel calculation of electron multiple scattering using Lanczos algorithms. *Phys. Rev. B* **2002**, *65* (10), 104107.
(52) Locock, A. J.; Burns, P. C. Crystal structures and synthesis of the copper-dominant members of the autunite and meta-autunite groups: Torbernite, zeunerite, metatorbernite and metazeunerite. *Can. Mineral.* **2003**, *41* (2), 489.
(53) Catalano, J. G.; Brown, G. E. Uranyl adsorption onto montmorillonite: Evaluation of binding sites and carbonate complexation. *Geochim. Cosmochim. Acta* **2005**, *69* (12), 2995−3005.
(54) Foerstendorf, H.; Heim, K.; Rossberg, A. The complexation of uranium(VI) and atmospherically derived CO_2 at the ferrihydrite−water interface probed by time-resolved vibrational spectroscopy. *J. Colloid Interface Sci.* **2012**, *377* (1), 299−306.
(55) Bargar, J. R.; Reitmeyer, R.; Lenhart, J. J.; Davis, J. A. Characterization of U(VI)-carbonato ternary complexes on hematite: EXAFS and electrophoretic mobility measurements. *Geochim. Cosmochim. Acta* **2000**, *64* (16), 2737−2749.
(56) Hiemstra, T.; Riemsdijk, W. H. V.; Rossberg, A.; Ulrich, K.-U. A surface structural model for ferrihydrite II: Adsorption of uranyl and carbonate. *Geochim. Cosmochim. Acta* **2009**, *73* (15), 4437−4451.
(57) Sivaswamy, V.; Boyanov, M. I.; Peyton, B. M.; Viamajala, S.; Gerlach, R.; Apel, W. A.; Sani, R. K.; Dohnalkova, A.; Kemner, K. M.; Borch, T. Multiple mechanisms of uranium immobilization by *Cellulomonas* sp. strain ES6. *Biotechnol. Bioeng.* **2011**, *108* (2), 264−276.
(58) Ray, A. E.; Bargar, J. R.; Sivaswamy, V.; Dohnalkova, A. C.; Fujita, Y.; Peyton, B. M.; Magnuson, T. S. Evidence for multiple modes of uranium immobilization by an anaerobic bacterium. *Geochim. Cosmochim. Acta* **2011**, *75* (10), 2684−2695.
(59) Sharp, J. O.; Lezama-Pacheco, J. S.; Schofield, E. J.; Junier, P.; Ulrich, K.-U.; Chinni, S.; Veeramani, H.; Margot-Roquier, C.; Webb, S. M.; Tebo, B. M.; Giammar, D. E.; Bargar, J. R.; Bernier-Latmani, R. Uranium speciation and stability after reductive immobilization in aquifer sediments. *Geochim. Cosmochim. Acta* **2011**, *75* (21), 6497−6510.
(60) Bernier-Latmani, R.; Veeramani, H.; Vecchia, E. D.; Junier, P.; Lezama-Pacheco, J. S.; Suvorova, E. I.; Sharp, J. O.; Wigginton, N. S.; Bargar, J. R. Non-uraninite products of microbial U(VI) reduction. *Environ. Sci. Technol.* **2010**, *44* (24), 9456−9462.
(61) Veeramani, H.; Alessi, D. S.; Suvorova, E. I.; Lezama-Pacheco, J. S.; Stubbs, J. E.; Sharp, J. O.; Dippon, U.; Kappler, A.; Bargar, J. R.; Bernier-Latmani, R. Products of abiotic U (VI) reduction by biogenic magnetite and vivianite. *Geochim. Cosmochim. Acta* **2011**, *75*, 2512−2528.
(62) Humphrey, W.; Dalke, A.; Schulten, K. VMD—Visual Molecular Dynamics. *J. Mol. Graphics* **1996**, *14*, 33−38.